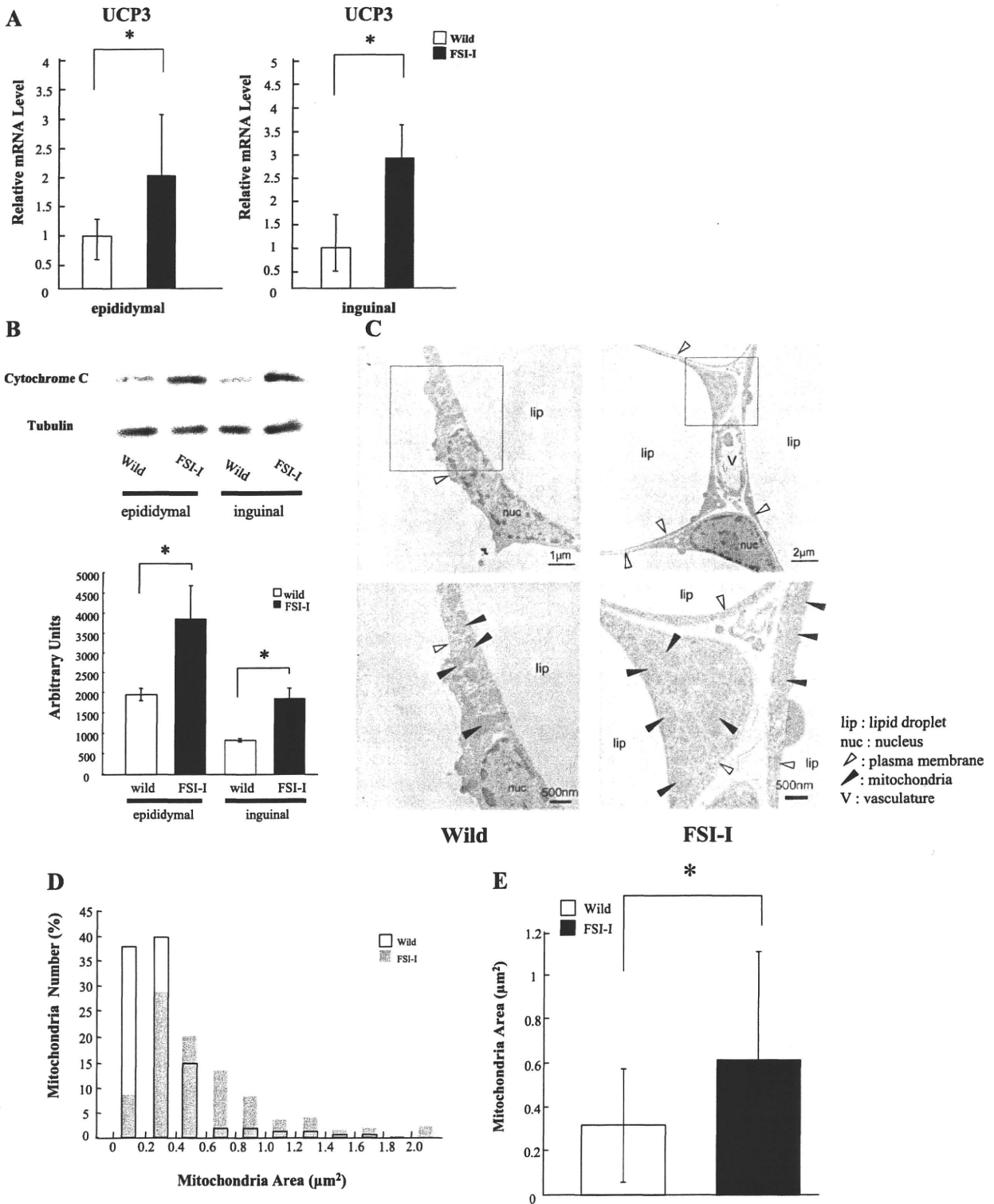


and by scanning electron microscopy (Fig. 1C). Both techniques confirmed that adipocyte size was smaller in FS I-I Tg mice than in wild-type mice. Therefore, we determined the mean adipocyte area. Quantification of the area of

individual adipocytes is shown in Fig. 1D. At week 20 of age, the mean adipocyte area was smaller in FS I-I Tg mice than in wild-type mice (436.8 ± 309.1 vs. $717.4 \pm 579.1 \mu\text{m}^2$, respectively; Fig. 1D). These results indicate that FS



I-I Tg mice showed less fat accumulation than wild-type mice when fed a NFD.

Changes in expression of metabolic molecules in FS I-I Tg mice. We examined the expression levels of mRNAs encoding the UCPs, proteins expressed on the inner membrane of the mitochondria that uncouple the proton gradient from ATP synthesis and are implicated in thermogenesis (7). The expression levels of UCP3 in epididymal and inguinal adipose tissues were increased two- and threefold, respectively, in FS I-I Tg mice compared with wild-type mice (Fig. 2A). However, the expression levels of UCP1 and UCP2 mRNAs in adipose tissues in FS I-I Tg mice and wild-type mice were comparable (data not shown).

We next quantified the abundance of mitochondria in adipose tissues by using the mitochondria marker cytochrome *c* (Fig. 2B). Consistent with the increase in UCP3 mRNA, the protein expression of cytochrome *c* was increased in the epididymal and inguinal fat pads in FS I-I Tg mice compared with wild-type mice (Fig. 2B). In skeletal muscle, cytochrome expression did not change (Suppl. Fig. S1; supplementary materials are found with the online version of this paper on the Journal website). We also determined mitochondria size by transmission electron microscopy (Figs. 2, C and D, and S2), which revealed that both the number and size of mitochondria in adipocytes were increased in FS I-I Tg mice compared with wild-type mice. These results raise the interesting possibility that FS I-I Tg mice exhibit increased energy metabolism and/or energy partitioning between adipose tissue and skeletal muscle.

Expression of FS I-I and altered Smad 3 phosphorylation in FS I-I Tg mice. To ascertain that FS I-I expression is restricted in skeletal muscle, we performed Western blotting using skeletal muscle, liver, adipose tissues and serum from wild-type and FS I-I Tg mice. As shown in Fig. 3A, FS I-I protein was expressed in skeletal muscle, but was not detected in either liver or adipose tissues. In serum, follistatin was detected, whereas FS I-I was hardly detectable. Next, we studied the phosphorylation of Smad 3 protein by immunoblotting. As shown in Fig. 3B, Smad 3 phosphorylation in skeletal muscle from FS I-I Tg mice was significantly reduced compared with that from control mice. In other tissues such as liver and adipose tissues, Smad 3 phosphorylation was either undetectable or unchanged.

FS I-I Tg mice are resistant to HFD-induced obesity. We previously reported that NFD-fed FS I-I Tg mice exhibited greater weight gain than wild-type mice between 6 and 15 wk of age, even though food intakes were comparable (27). Here, the FS I-I Tg and wild-type mice were fed a HFD from weeks 4 to 13 of age to induce obesity. Interestingly, weight gain did not differ between FS I-I Tg and wild-type mice (Fig. 4A). However, the weight of adipose tissue depots was lower in FS I-I Tg mice than in wild-type mice, being 25.0 and 34.3%

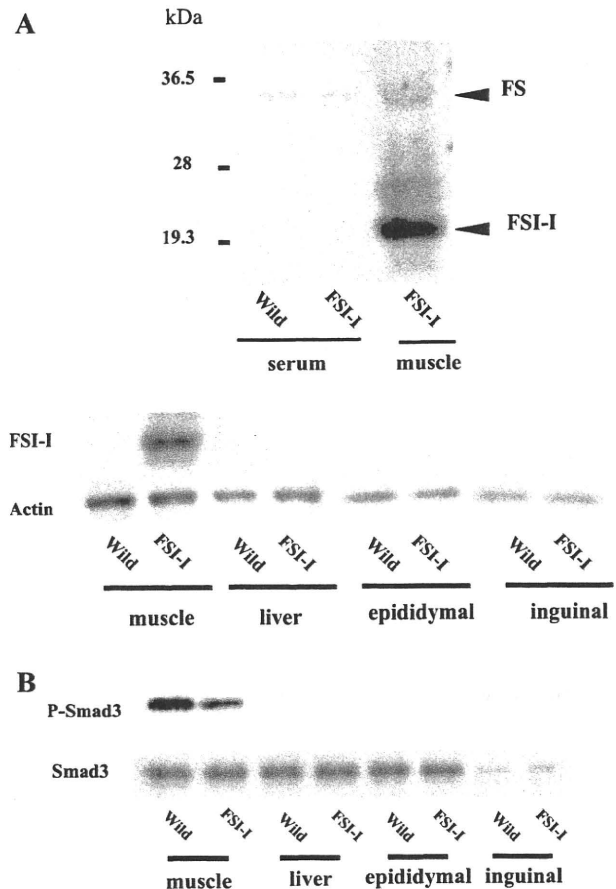


Fig. 3. A: detection of FS and FS I-I in serum, femoris skeletal muscle (Qf), liver, and fats. FS is detected as 33-kDa protein in serum, whereas FS I-I is not detectable in serum in FS I-I Tg mice (top). FS I-I is detected in skeletal muscle but not in liver or fats (bottom). B: detection of phosphorylated Smad3 in skeletal muscle, liver, and epididymal and inguinal fats. In quadriceps skeletal muscle (Qf) of FS I-I Tg mice, phosphorylated Smad 3 is reduced compared with that of wild-type mice. Smad 3 antibody was used as a loading control. In other tissues, phosphorylation of Smad 3 is either undetectable or unchanged.

lower for the inguinal and retroperitoneal fat pads, respectively (Fig. 4B). By contrast, FS I-I Tg mice exhibited increased muscle weight, as the TA, EDL, Qf, and soleus muscles were 43, 45, 21, and 27% higher in FS I-I Tg mice than in wild-type mice (Fig. 4C). Thus, the absence of a difference in body weight gain between wild-type mice and FS I-I Tg mice fed the HFD was attributed to changes of adipose tissue, muscle, and liver weights in FS I-I Tg mice (see Figs. 4, B and C, and 5B).

We next measured serum parameters, including triglyceride, NEFA, total cholesterol, insulin, leptin, and adiponectin levels

Fig. 2. A: relative mRNA expression of UCP3 in epididymal and inguinal adipose tissues in wild-type and FS I-I Tg mice. Adipose tissues from 5 mice each for wild-type and FS I-I Tg mice were used and quantitated. UCP3 mRNA expression levels were quantified by RT-PCR. * $P < 0.05$, Student's *t*-test. B: protein expression of cytochrome *c* in epididymal and inguinal fat pads from wild-type and FS I-I Tg mice. Cytochrome *c* was detected at 14 kDa. Tubulin expression was used as a loading control (top). Adipose tissues from 3 mice each for wild-type and FS I-I Tg mice were used and quantitated. * $P < 0.02$, Student's *t*-test (bottom). C: transmission electron microscopy of epididymal adipose tissues from 20-wk-old wild-type and FS I-I Tg mice. Higher magnification views of indicated regions (squares) at top are shown at bottom. Scale bars, 1 μm in top left, 2 μm in top right, and 500 nm in bottom. Lip, lipid droplet; nuc, nucleus; white arrowheads, plasma membranes; black arrowheads, mitochondria; V, vasculature. D: analysis of mitochondria size and number from wild-type and FS I-I Tg mice. One hundred fifty mitochondria of epididymal adipocytes each from 3 wild-type and FS I-I Tg mice were analyzed and plotted. E: mean mitochondria areas of wild-type and FS I-I Tg mice. * $P < 0.001$, Student's *t*-test.

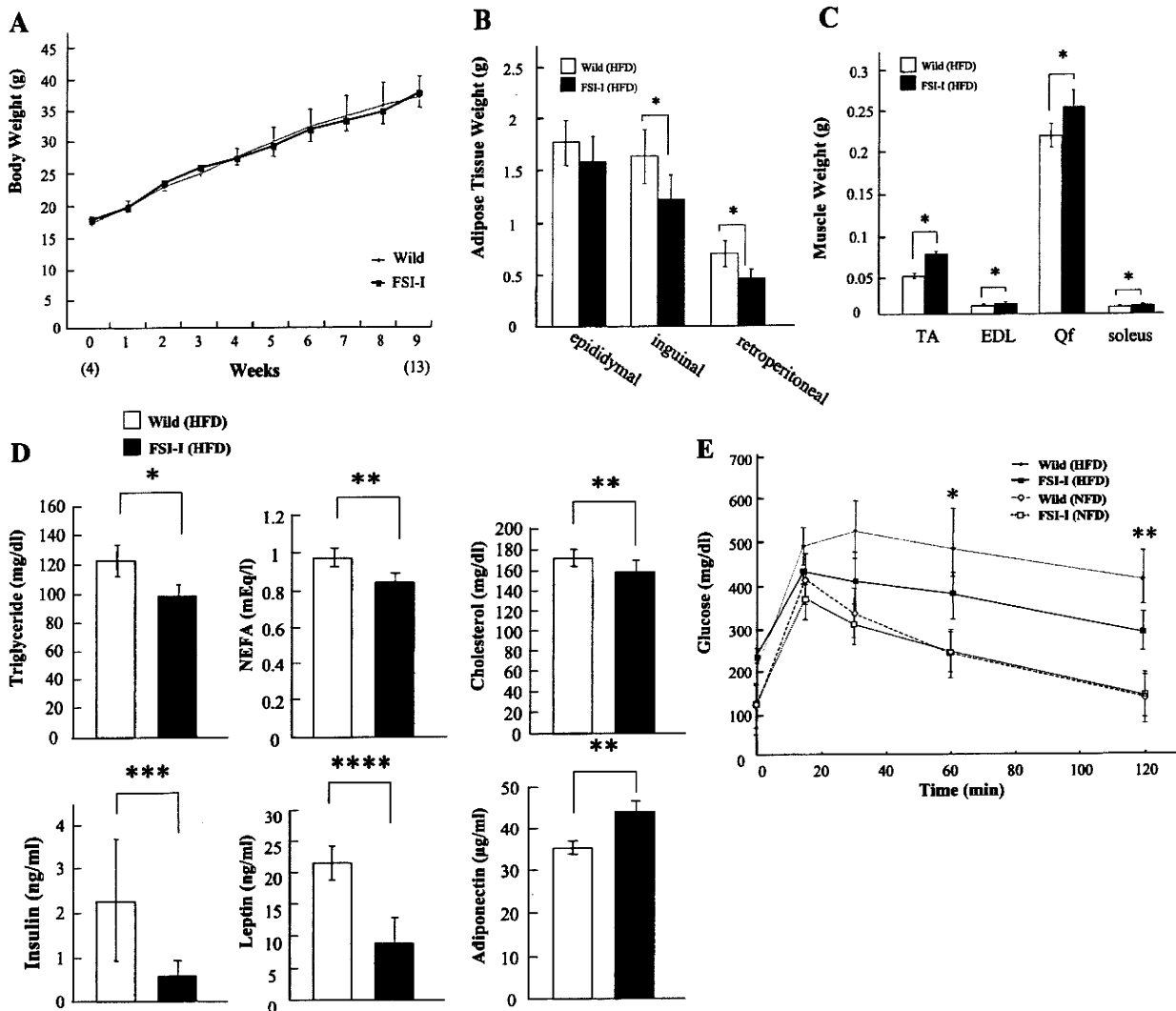


Fig. 4. A: body weights (g) of wild-type and FS I-I Tg mice fed a high-fat diet (HFD) from 4 to 13 wk of age; $n = 5$ mice per group. B: weight of epididymal, inguinal, and retroperitoneal fat pads of wild-type and FS I-I Tg mice fed HFD from 4 to 13 wk of age. $*P < 0.05$, Student's t -test; $n = 5$ –6 mice per group. C: weights of the tibialis anterior (TA), extensor digitorum longus (EDL), quadriceps femoris (QF), and soleus muscles from wild-type and FS I-I Tg mice fed a HFD from 4 to 13 wk of age. $*P < 0.005$, Student's t -test; $n = 5$ mice per group. D: triglycerides, NEFA, cholesterol, insulin, leptin, and adiponectin levels in wild-type and FS I-I Tg mice fed HFD from 4 to 13 wk of age. $*P < 0.0005$, $**P < 0.003$, $***P < 0.05$, $****P < 0.007$, Student's t -test; $n = 4$ –6 mice per group. E: glucose tolerance test in wild-type and FS I-I Tg mice fed either normal diet (NFD) or HFD from 4 to 13 wk of age. Blood glucose was measured at 0, 15, 30, 60, and 120 min after glucose (dextrose) injection; $n = 6$ –8 mice per group. $*P < 0.05$ and $**P < 0.01$, Student's t -test.

in FS I-I Tg and wild-type mice (Fig. 4D). Of note, triglyceride, NEFA, cholesterol, and leptin levels were lower in FS I-I Tg mice by 19.7, 13.6, 7.7, and 58.4%, respectively, compared with wild-type mice (Fig. 4B and Table 1). However, the serum adiponectin levels were 25.7% higher in FS I-I Tg mice than in wild-type mice when fed the HFD. By contrast, there were no significant differences in triglyceride, NEFA, cholesterol, leptin, and adiponectin levels between NFD-fed FS I-I Tg and wild-type mice (Table 1).

Defects in glucose homeostasis are important factors involved in the development of obesity. Therefore, we measured whole body glucose tolerance in FS I-I and wild-type mice fed the NFD or the HFD. Although there were no differences between NFD-fed FS I-I and wild-type mice, the glucose level

tended to be lower in HFD-fed FS I-I Tg mice than in HFD-fed wild-type mice (Fig. 4E). These results indicate that the response to diet-induced obesity differs between FS I-I Tg and wild-type mice. In the NFD condition, no difference was observed in insulin tolerance (data not shown). However, in the HFD condition, FS I-I Tg mice exhibited better insulin tolerance than wild-type mice (Fig. S3).

FS I-I Tg mice are resistant to HFD-induced hepatic steatosis. As expected, the HFD increased hepatocyte lipid content and induced hepatic steatosis in wild-type mice. However, hepatic steatosis was not observed in HFD-fed FS I-I Tg mice (Fig. 5A). The liver from FS I-I Tg mice was histologically normal, even when these mice were fed the HFD, and showed significantly less lipid accumulation than HFD-fed

Table 1. Serum metabolic parameters in wild-type and FS I-I Tg mice fed NFD or HFD

Diet Treatment Genotype	NFD		HFD	
	Wild Type	FSI-I Tg	Wild Type	FSI-I Tg
Triglyceride, mg/dl	108.5 ± 10.3	101.1 ± 7.5	122.8 ± 10.6	98.6 ± 7.5 ^a
NEFA, mEq/l	0.83 ± 0.05	0.73 ± 0.09	0.97 ± 0.05	0.84 ± 0.04 ^{b1}
Cholesterol, mg/dl	91.8 ± 4.9	81.2 ± 1.7	170.8 ± 7.7	157.6 ± 10.7 ^{b2}
Fasting glucose, mg/dl	101.2 ± 16.2	107.8 ± 14.7	208.0 ± 2.0	208.0 ± 6.6
Insulin, ng/ml	0.91 ± 0.13	0.51 ± 0.12 ^{b4}	2.16 ± 1.56	0.58 ± 0.34 ^c
Leptin, ng/ml	4.00 ± 0.41	3.88 ± 0.14	21.35 ± 2.74	8.90 ± 3.88 ^d
Adiponectin, µg/ml	21.0 ± 1.2	20.4 ± 1.3	35.1 ± 1.6	44.0 ± 2.4 ^{b3}

Values are means ± SD; *n* = 4–6 mice per group. NFD, normal fat diet; HFD, high-fat diet; FSI I-I Tg, follistatin-derived peptide transgenic. a, b1–b3, c, and d, vs. wild-type mice (HFD); b4, vs. wild-type mice (NFD). ^a*P* < 0.0005; ^{b1–b4}*P* < 0.003; ^c*P* < 0.05; ^d*P* < 0.007 (Student's *t*-test).

wild-type mice (Fig. 5A). In addition, hepatic steatosis did not develop even in aged mice in FS I-I Tg mice (data not shown). The weight of the liver in HFD-fed FS I-I Tg mice was 13% less than that of wild-type mice (Fig. 5, A and B). The lower liver weight in FS I-I mice was attributed to reduced hepatocyte triglyceride accumulation in these mice compared with wild-type mice (Fig. 5C). Triglyceride contents in skeletal muscle were not significantly different between FS I-I mice and wild-type mice fed the HFD in our experimental condition (data not shown).

We next performed qPCR to determine the mRNA expression of genes related to fatty acid synthesis, including SCD1, which is required for the biosynthesis of monounsaturated fatty acids such as oleic acid and plays a key role in the hepatic synthesis of triglycerides (25). The hepatic SCD1 mRNA expression levels were 20% lower in HFD-fed FS I-I Tg mice than in wild-type mice (Fig. 6A). By contrast, the mRNA expression of ACC1 mRNA did not differ between FS I-I Tg and wild-type mice. We also measured the mRNA expression levels of Gck and PFK, two enzymes that regulate the glycolytic pathway. The expression levels of both genes were increased in FS I-I Tg mice compared with wild-type mice, 1.8-fold for GcK and 2-fold for PFK (Fig. 6A).

We measured hepatic fatty acid content in FS I-I Tg and wild-type mice. Interestingly, in HFD-fed mice, the fatty acid content and the ratio of fatty acids differed between the FS I-I Tg and wild-type mice. For example, the livers from HFD-fed FS I-I Tg mice showed an increased stearyl acid (C18:0) ratio and decreased oleic acid (C18:1) ratio to the total fatty acid content (Fig. 6B and Table 2). The absolute content of oleic acid (C18:1) and palmitoleic acid (C16:1) did not increase in FS I-I Tg mice compared with wild-type mice (Table 2). This finding is consistent with the decreased mRNA level of SCD1. Taken together, these results indicate that FS I-I Tg mice were resistant to hepatic steatosis induced by HFD and had reduced monounsaturated fatty acid content, particularly oleic acid (C18:1) and palmitoleic acid (C16:1).

DISCUSSION

Inhibition of myostatin is useful for various muscular diseases, including muscular dystrophies, muscular atrophy, cachexia induced by cancer, and sarcopenia (19, 34, 38). Furthermore, myostatin-null mice and myostatin propeptide-overexpressing Tg mice were used to study the effects of myostatin inhibition on obesity (10, 14, 24, 41, 42). These studies revealed that the inhibition of myostatin decreased adipose tissue accumulation and improved diet-induced obesity and

genetic diabetes/obesity. The loss of myostatin in genetically obese mice partially suppressed adipose tissue accumulation and improved glucose metabolism (24). Meanwhile, upon high-fat feeding, the myostatin propeptide Tg mice showed favorable fat utilization and beneficial interactions between skeletal muscle and adipose tissues compared with control mice (42). Recent studies have suggested that inhibiting myostatin in muscle but not in adipose tissues is responsible for the decreased fat mass and improved insulin sensitivity (13). Indeed, inhibition of myostatin signaling in adipose tissue by Δ ACVR2B had no effect on body composition, weight gain, or insulin tolerance either on NFD or on HFD. By contrast, inhibition of myostatin by Δ ACVR2B in skeletal muscle resulted in increased lean mass, decreased fat mass, and improved glucose metabolism in mice fed an NFD or an HFD (13).

In our previous study, we reported the development and characterization of a novel myostatin inhibitor derived from follistatin, designated FS I-I. Although FS I-I showed significantly weaker inhibitory effects on activin, FS I-I retained its inhibitory effect on myostatin. In FS I-I Tg mice, inhibition of myostatin activity by FS I-I increased skeletal muscle mass and strength (27). Cardiac weight did not increase in FS I-I mice (Fig. S5). In this study, we have further demonstrated that Tg expression of the myostatin inhibitor FS I-I also has an anti-obesity effect and improved glucose tolerance and prevents hepatic steatosis induced by HFD.

Various strategies can be exploited to inhibit myostatin, including neutralizing monoclonal myostatin antibodies, myostatin propeptide and Δ ACVR2B (19). The neutralizing antibody is effective, but it can cause anti-idiotypic immunity after *in vivo* administration. The myostatin propeptide is susceptible to proteolytic cleavage by members of the bone morphogenetic protein (BMP)-1/tolloid family of metalloproteinases, impairing its ability to inhibit myostatin (40). Purified follistatin has several cleaved isoforms; the COOH-terminal region is susceptible to proteinase cleavage, although the cleaved follistatin molecules can still inhibit activin and myostatin (36). FS I-I comprises the NH₂-terminal region and two consecutive follistatin domain I regions. Therefore, FS I-I lacks the native follistatin COOH-terminal region, which is susceptible to protease cleavage. Furthermore, follistatin is a naturally occurring peptide and may cause fewer immune responses than exogenous antibodies. Therefore, among myostatin inhibitors, FS I-I offers some advantages over monoclonal antibodies and myostatin propeptide.

Adipocytes in FS I-I Tg mice contained fewer lipids than wild-type mice when they were fed a standard diet. Therefore,

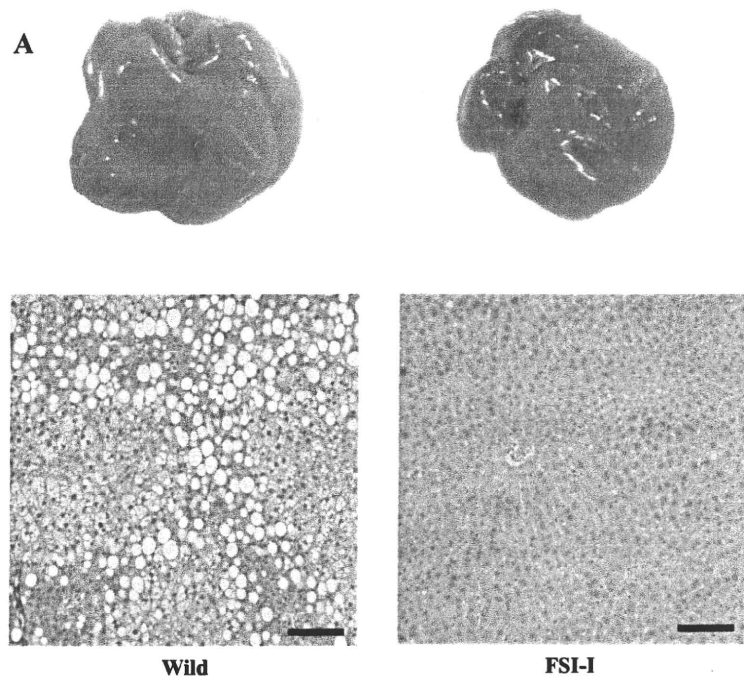
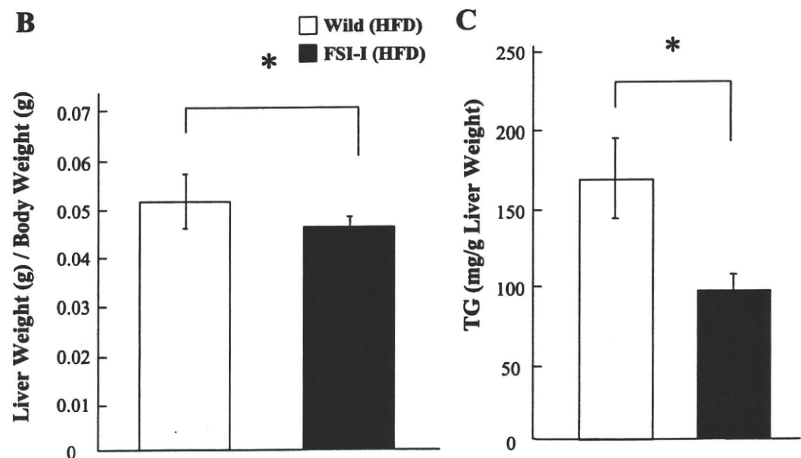


Fig. 5. A: morphology of liver samples from 13-wk-old wild-type and FS I-I Tg fed HFD. Liver sections were analyzed with H&E staining (*bottom*). Scale bar, 100 μ m. B: relative liver weight (g) to body weight (g) of wild-type and FS I-I Tg mice fed HFD from 4 to 13 wk of age; $n = 6$ mice per group. $*P < 0.01$, Student's *t*-test. C: hepatic triglyceride (TG) content in wild-type and FS I-I Tg mice fed HFD from 4 to 13 wk of age; $n = 5$ mice per group. $*P < 0.0005$, Student's *t*-test.



mean adipocyte size was smaller in FS I-I Tg mice than in wild-type mice (Fig. 1, B–D). By contrast, fat mass was normal in myostatin propeptide Tg mice fed a standard diet (42). During HFD feeding, myostatin knockout mice gained fat mass, whereas muscle weight was unaffected by the HFD. By contrast, in FS I-I Tg mice, the skeletal muscle mass was still increased, albeit blunted compared with control mice (27, 42). The differences in the increases of fat and skeletal muscle mass in these models might be due to how much endogenous active myostatin is present *in vivo*.

We examined the expression levels of mRNAs encoding UCPs. The adipose tissue in FS I-I Tg mice showed upregulation of UCP3 mRNA expression levels (Fig. 2A) but not UCP1 or UCP2 compared with wild-type mice (data not

shown). While UCP2 shows rather ubiquitous expression, UCP1 is specifically expressed in brown adipocytes and UCP3 is specifically expressed in skeletal muscle, brown adipose tissues, and heart (6, 18). Upregulation of UCP3 mRNA expression levels in FS I-I Tg mice was thought to increase energy expenditure. In addition, we observed adipose tissue by transmission electron microscopy (Fig. 2C). We found that the adipocytes in FS I-I Tg mice contained increased numbers of mitochondria. The mitochondria in FS I-I Tg adipocyte contained mitochondrial cristae, suggesting that they had normal mitochondrial function. To our knowledge, this is the first report demonstrating that myostatin inhibition causes an apparent increase in mitochondria abundance. The biogenesis of mitochondria requires coordinated protein synthesis and as-

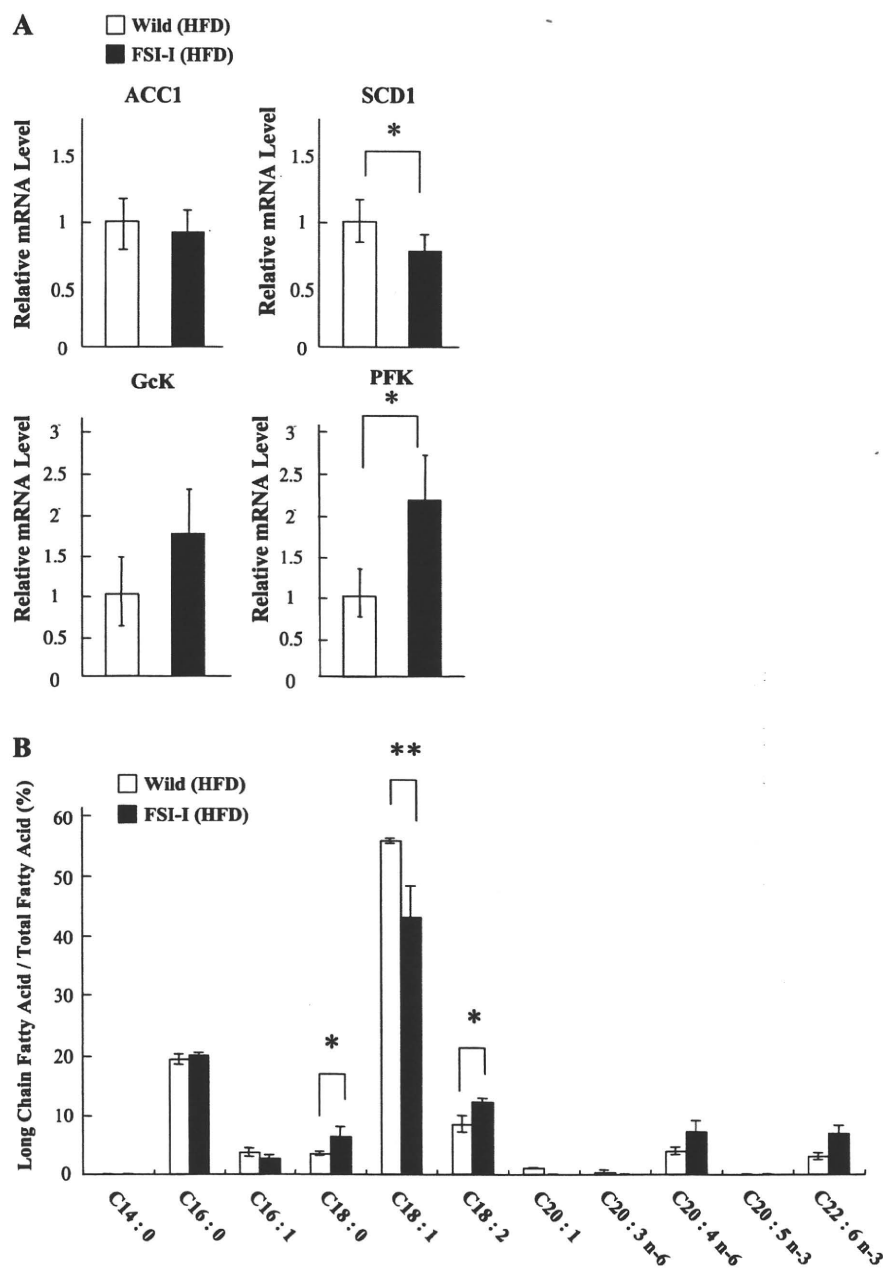


Fig. 6. A: relative hepatic mRNA expression levels of ACC1, SCD1, Gck, and PFK were measured by qPCR in wild-type and FS I-I Tg mice fed HFD; $n = 5$ mice per group. * $P < 0.05$, Student's *t*-test. B: ratio of long-chain fatty acids to total fatty acids in liver of wild-type and FS I-I Tg mice fed HFD; $n = 6$ mice per group. * $P < 0.05$ and ** $P < 0.03$, Student's *t*-test.

sembly from both the nuclear and mitochondrial genomes. Mitochondrial abundance can be modulated in response to physical activity, metabolic demands, and nutrition (16). PPAR γ ligands increase mitochondrial biogenesis in white adipose tissue, and the PPAR γ coactivator-1 (PGC-1) family is well characterized as a pivotal transcriptional coactivator for mitochondrial biogenesis (16). Although the mechanism of how mitochondria number and size are increased in adipocytes of FS I-I Tg mice remains to be determined, one possible mechanism may be upregulation of the PGC-1-dependent transcription cascade in white adipose tissues. Alternatively, it is also possible that the rate of mitochondrial turnover could be changed in white adipocytes of FS I-I Tg mice. Energy expen-

diture in FS I-I Tg mice was influenced by increased muscle mass, whereas adipose tissue is involved in energy storage. Therefore, changes in mitochondria abundance in adipocytes could modulate whole body energy expenditure and storage.

The insulin level in HFD-fed FS I-I Tg mice was lower than that in control mice (Fig. 4D), but glucose tolerance was better in HFD-fed FS I-I Tg mice than in HFD-fed wild-type mice. FS I-I is expressed under a skeletal muscle-specific myosin light-chain promoter and shows a widespread increase in muscle mass. The expression of FS I-I is restricted to skeletal muscles and is not detected in adipose tissues, liver, or serum (Fig. 3A). The circulating level of FS I-I in serum is under the detection limit and low compared with that of follistatin.

Table 2. Hepatic fatty acid in wild-type and FS I-I Tg mice fed NFD or HFD

Diet Treatment Genotype	NFD		HFD	
	Wild Type	FSI-I Tg	Wild Type	FSI-I Tg
C14:0	ND	ND	ND	ND
C16:0	13.1 ± 7.2	10.5 ± 4.9	20.2 ± 4.9	10.5 ± 2.8 ^{a1}
C16:1	2.1 ± 1.7	1.3 ± 0.9	3.8 ± 1.1	1.5 ± 0.6 ^{a2}
C18:0	3.0 ± 0.4	3.3 ± 1.0	3.5 ± 0.4	3.2 ± 0.1
C18:1	27.1 ± 22.1	21.4 ± 17.3	57.8 ± 12.0	23.1 ± 9.4 ^b
C18:2	7.2 ± 2.1	6.7 ± 2.0	8.9 ± 2.7	6.4 ± 1.5
C20:1	0.3 ± 0.5	ND	1.1 ± 0.2	ND
C20:3n-6	0.1 ± 0.2	0.1 ± 0.2	0.4 ± 0.3	ND
C20:4n-6	3.0 ± 1.0	3.4 ± 1.5	3.9 ± 0.2	3.6 ± 0.1
C22:6n-3	3.4 ± 0.9	3.6 ± 1.0	3.1 ± 0.7	3.5 ± 0.3
Total	59.3 ± 35.9	50.3 ± 28.1	102.7 ± 22	51.8 ± 14.9

Values are means ± SD; n = 6 mice per group. ND, not detected (μg/mg). a1–a2 and b, vs. wild-type mice (HFD); ^{a1–a2}P < 0.05; ^bP < 0.02 (Student's *t*-test).

Furthermore, a 30.2% reduction of phosphorylated Smad 3, representing lower myostatin signaling, was detected in skeletal muscles but not in other tissues (Fig. 3B). Therefore, it is likely that myostatin signaling in muscle, rather than the direct effects of myostatin on adipose tissue, is responsible for the decrease in fat mass in FS I-I Tg mice. We also studied the effects of myostatin and FS I-I in Hep G2 cells and 3T3-L1 cell lines. In both cases, the triglyceride level was not affected either by myostatin or by follistatin-derived peptide stimulation (Fig. S4), supporting the secondary and indirect effects of FS I-I on adipocytes and hepatocytes. The increased skeletal muscle mass may have greater capacity for glucose uptake, reducing substrate supply for hepatic lipogenesis.

The normal age-dependent adipose tissue accumulation was decreased in NFD-fed FS I-I Tg mice (Fig. 1A). Intriguingly, the adipocytes were smaller as a result of myostatin inhibition by FS I-I (Fig. 1, B–D), reflecting reduced lipid accumulation. Obesity occurs when the adipose tissue is overloaded with high-energy nutrients and energy expenditure is reduced. Therefore, we studied the effect of diet-induced obesity in FS I-I Tg and wild-type mice. The body weight of HFD-fed FS I-I Tg mice was comparable with that of HFD-fed wild-type mice (Fig. 4A), which was attributed to the increase in muscle weight and decrease in adipose tissue and liver weights in FS I-I Tg mice (Fig. 4, B and C). Interestingly, there is a report that mice with an insertion allele at the *Inhba* locus, *Inhba*^{BK}, are smaller and leaner than wild-type littermate (20). In *Inhba*^{BK} mice, the sequences of the mature activin-βA domain were replaced with the corresponding sequences from activin-βB. *Inhba*^{BK} mice have less adipose tissue than wild-type littermates. The growth of *Inhba*^{BK} is improved by providing an HFD to a level comparable with that of wild-type mice on an NFD (20). The phenotype of FS I-I mice with lower myostatin signaling is different from that of *Inhba*^{BK} mice. Therefore, although activin A and myostatin are functionally similar to maintain energy balance and regulate skeletal muscle mass, they may have different functions in vivo. As would be expected, the HFD increased the levels of cholesterol, fasting glucose, insulin, and leptin (Fig. 4D and Table 1) compared with the NFD in wild-type mice (Table 1). However, the triglyceride, NEFA, cholesterol, insulin, and leptin levels were lower in HFD-fed FS I-I Tg mice than in HFD-fed wild-type

mice (Table 1 and Fig. 4D). Furthermore, we observed an increase in serum adiponectin in FS I-I Tg mice (Table 1). These results are similar to those of myostatin-null mice and myostatin propeptide Tg mice (13, 42). Interestingly, the HFD-fed FS I-I Tg mice exhibited better glucose tolerance than HFD-fed wild type mice (Fig. 4E). By contrast, in mice fed the NFD, glucose tolerance was similar in FS I-I Tg and wild-type mice. This differs from the situation in myostatin knockout mice, because myostatin knockout mice showed improved glucose tolerance, even when they were fed the NFD (24). With respect to whole body metabolism, we performed indirect calorimetric analyses. Although food intake was not significantly different between wild-type and FS I-I mice, the metabolic rate calculated from $\dot{V}O_2$ was increased in FS I-I Tg compared with control. When normalized with body weight, no statistically significant difference was observed (Supplementary Table S1). Collectively, these results indicate that FS I-I Tg mice were resistant to HFD-induced obesity and showed improved glucose tolerance during excess energy intake.

Intriguingly, FS I-I Tg mice were resistant to hepatic steatosis during high-fat feeding, which was confirmed by histology, liver weight, and liver fatty acid accumulation (Fig. 5, A–C and Table 2). The hepatic histology of HFD-fed FS I-I Tg mice did not show any difference to NFD-fed wild-type mice. The hepatic expression level of SCD1 mRNA was lower in FS I-I Tg mice than in wild-type mice. SCD1 is a rate-limiting lipogenic enzyme required for the synthesis of monounsaturated fatty acids and plays a key role in the hepatic synthesis of triglycerides. As a result of decreased SCD1 expression, the hepatic content of oleic acid (C18:1) and palmitoleic acid (C16:1), monounsaturated fatty acids produced by SCD1, was decreased (Fig. 6B and Table 2). A decrease in SCD1 expression was reported to be responsible for the prevention of diet-induced obesity, insulin resistance, and diabetes (9, 28). Furthermore, SCD1-null mice were resistant to diet-induced obesity and hepatic steatosis (9). The resistance of FS I-I Tg mice to HFD-induced obesity and hepatic steatosis may, in part, involve the reduced mRNA expression of SCD1. Changes of RNA and protein end points represent lower adiposity and lower hepatic fat levels. The lower adiposity is likely secondary to increased muscle mass and lower myostatin signaling in skeletal muscle.

The increase in skeletal muscle mass and reduction in fat mass would likely take at least several months to occur. Meanwhile, injection of myostatin neutralizing antibody does not decrease the adipose tissue mass (35, 39). However, even if the fat mass is not decreased, it seems likely that the inhibition of myostatin improves glucose tolerance and insulin sensitivity and prevents hepatic steatosis due to lower insulin levels, increased adiponectin levels, and changes in substrate utilization in skeletal muscle, adipose tissue, and liver. In summary, the inhibition of myostatin by various strategies, including follistatin-derived peptide, may offer a novel therapy against obesity, diabetes, and hepatic steatosis.

ACKNOWLEDGMENTS

We thank Drs. K. Hitachi, A. Uezumi, and H. Ageta for discussion and advice. We also thank S. Sato and A. Yamaguchi for technical assistance.

GRANTS

This research was partly supported by a Grant-in-Aid for Scientific Research (21590320 to K. Tsuchida) from the Japan Society for the Promotion of Science, a Grant-in-Aid for Young Scientists (22790328 to M. Nakatani) from JSPS, a research grant (H20-018) on psychiatric and neurological diseases and mental health from the Ministry of Health, Labour and Welfare, and an Intramural Research Grant (20B-13) for Neurological and Psychiatric Disorders of National Center of Neurology and Psychiatry.

DISCLOSURES

No conflicts of interest are reported by the authors.

REFERENCES

- Akpan I, Goncalves MD, Dhir R, Yin X, Pistilli EE, Bogdanovich S, Khurana TS, Ucran J, Lachey J, Ahima RS. The effects of a soluble activin type IIB receptor on obesity and insulin sensitivity. *Int J Obes (Lond)* 33: 1265–1273, 2009.
- Amthor H, Nicholas G, McKinnell I, Kemp CF, Sharma M, Kambadur R, Patel K. Follistatin complexes Myostatin and antagonises Myostatin-mediated inhibition of myogenesis. *Dev Biol* 270: 19–30, 2004.
- Archibald FM, Skipski VP. Determination of fatty acid content and composition in ultramicro lipid samples by gas-liquid chromatography. *J Lipid Res* 7: 442–445, 1966.
- Bligh EG, Dyer WJ. A rapid method of total lipid extraction and purification. *Can J Biochem Physiol* 37: 911–917, 1959.
- Boman IA, Klemetsdal G, Blichfeldt T, Nafstad O, Vage DI. A frameshift mutation in the coding region of the myostatin gene (MSTN) affects carcass conformation and fatness in Norwegian White Sheep (*Ovis aries*). *Anim Genet* 40: 418–422, 2009.
- Brand MD, Esteves TC. Physiological functions of the mitochondrial uncoupling proteins UCP2 and UCP3. *Cell Metab* 2: 85–93, 2005.
- Chan CB, Harper ME. Uncoupling proteins: role in insulin resistance and insulin insufficiency. *Curr Diabetes Rev* 2: 271–283, 2006.
- Clop A, Marcq F, Takeda H, Pirottin D, Tordoir X, Bibe B, Bouix J, Caiment F, Elsen JM, Eycheffe F, Larzul C, Laville E, Meish F, Milenkovic D, Tobin J, Charlier C, Georges M. A mutation creating a potential illegitimate microRNA target site in the myostatin gene affects muscularity in sheep. *Nat Genet* 38: 813–818, 2006.
- Dobrzyn A, Ntambi JM. Stearoyl-CoA desaturase as a new drug target for obesity treatment. *Obes Rev* 6: 169–174, 2005.
- Feldman BJ, Streepers RS, Farese RV Jr, Yamamoto KR. Myostatin modulates adipogenesis to generate adipocytes with favorable metabolic effects. *Proc Natl Acad Sci USA* 103: 15675–15680, 2006.
- Gamer LW, Cox KA, Small C, Rosen V. Gdf11 is a negative regulator of chondrogenesis and myogenesis in the developing chick limb. *Dev Biol* 229: 407–420, 2001.
- Gilson HM, Schakman OR, Kalista S, Lause P, Tsuchida K, Thissen JP. Follistatin induces muscle hypertrophy through satellite cell proliferation and inhibition of both myostatin and activin. *Am J Physiol Endocrinol Metab* 297: E157–E164, 2009.
- Guo T, Jou W, Chanturiya T, Portas J, Gavrilova O, McPherron AC. Myostatin inhibition in muscle, but not adipose tissue, decreases fat mass and improves insulin sensitivity. *PLoS One* 4: e4937, 2009.
- Hamrick MW, Pennington C, Webb CN, Isaacs CM. Resistance to body fat gain in “double-muscled” mice fed a high-fat diet. *Int J Obes (Lond)* 30: 868–870, 2006.
- Hill JJ, Davies MV, Pearson AA, Wang JH, Hewick RM, Wolfman NM, Qiu Y. The myostatin propeptide and the follistatin-related gene are inhibitory binding proteins of myostatin in normal serum. *J Biol Chem* 277: 40735–40741, 2002.
- Hock MB, Kralli A. Transcriptional control of mitochondrial biogenesis and function. *Annu Rev Physiol* 71: 177–203, 2009.
- Ishigaki Y, Katagiri H, Yamada T, Ogihara T, Imai J, Uno K, Hasegawa Y, Gao J, Ishihara H, Shimosegawa T, Sakoda H, Asano T, Oka Y. Dissipating excess energy stored in the liver is a potential treatment strategy for diabetes associated with obesity. *Diabetes* 54: 322–332, 2005.
- Krauss S, Zhang CY, Lowell BB. The mitochondrial uncoupling-protein homologues. *Nat Rev Mol Cell Biol* 6: 248–261, 2005.
- Lee SJ. Regulation of muscle mass by myostatin. *Annu Rev Cell Dev Biol* 20: 61–86, 2004.
- Li L, Shen JJ, Bournat JC, Huang L, Chattopadhyay A, Li Z, Shaw C, Graham BH, Brown CW. Activin signaling: effects on body composition and mitochondrial energy metabolism. *Endocrinology* 150: 3521–3529, 2010.
- McPherron AC, Huynh TV, Lee SJ. Redundancy of myostatin and growth/differentiation factor 11 function. *BMC Dev Biol* 9: 24, 2009.
- McPherron AC, Lawler AM, Lee SJ. Regulation of skeletal muscle mass in mice by a new TGF-beta superfamily member. *Nature* 387: 83–90, 1997.
- McPherron AC, Lee SJ. Double muscling in cattle due to mutations in the myostatin gene. *Proc Natl Acad Sci USA* 94: 12457–12461, 1997.
- McPherron AC, Lee SJ. Suppression of body fat accumulation in myostatin-deficient mice. *J Clin Invest* 109: 595–601, 2002.
- Miyazaki M, Flowers MT, Sampath H, Chu K, Otzelberger C, Liu X, Ntambi JM. Hepatic stearoyl-CoA desaturase-1 deficiency protects mice from carbohydrate-induced adiposity and hepatic steatosis. *Cell Metab* 6: 484–496, 2007.
- Mosher DS, Quignon P, Bustamante CD, Sutter NB, Mellersh CS, Parker HG, Ostrander EA. A mutation in the myostatin gene increases muscle mass and enhances racing performance in heterozygote dogs. *PLoS Genet* 3: e79, 2007.
- Nakatani M, Takehara Y, Sugino H, Matsumoto M, Hashimoto O, Hasegawa Y, Murakami T, Uezumi A, Takeda S, Noji S, Sunada Y, Tsuchida K. Transgenic expression of a myostatin inhibitor derived from follistatin increases skeletal muscle mass and ameliorates dystrophic pathology in mdx mice. *FASEB J* 22: 477–487, 2008.
- Ntambi JM, Miyazaki M. Recent insights into stearoyl-CoA desaturase-1. *Curr Opin Lipidol* 14: 255–261, 2003.
- Ohsawa Y, Hagiwara H, Nakatani M, Yasue A, Moriyama K, Murakami T, Tsuchida Noji S K, Sunada Y. Muscular atrophy of caveolin-3-deficient mice is rescued by myostatin inhibition. *J Clin Invest* 116: 2924–2934, 2006.
- Pangas SA, Jorgez CJ, Tran M, Agno J, Li X, Brown CW, Kumar TR, Matzuk MM. Intraovarian activins are required for female fertility. *Mol Endocrinol* 21: 2458–2471, 2007.
- Saito S, Sugino K, Yamanouchi K, Kogawa K, Titani K, Shiota K, Takahashi M, Sugino H. Characterization of antisera directed against follistatin/activin-binding protein peptides. *Endocrinol Jpn* 38: 377–382, 1991.
- Schuelke M, Wagner KR, Stolz LE, Hubner C, Riebel T, Komen W, Braun T, Tobin JF, Lee SJ. Myostatin mutation associated with gross muscle hypertrophy in a child. *N Engl J Med* 350: 2682–2688, 2004.
- Shelton GD, Engvall E. Gross muscle hypertrophy in whippet dogs is caused by a mutation in the myostatin gene. *Neuromuscul Disord* 17: 721–722, 2007.
- Siriect V, Salerno MS, Berry C, Nicholas G, Bower R, Kambadur R, Sharma M. Antagonism of myostatin enhances muscle regeneration during sarcopenia. *Mol Ther* 15: 1463–1470, 2007.
- Stolz LE, Li D, Qadri A, Jalenak M, Klamann LD, Tobin JF. Administration of myostatin does not alter fat mass in adult mice. *Diabetes Obes Metab* 10: 135–142, 2008.
- Sugino K, Kurosawa N, Nakamura T, Takio K, Shimasaki S, Ling N, Titani K, Sugino H. Molecular heterogeneity of follistatin, an activin-binding protein. Higher affinity of the carboxyl-terminal truncated forms for heparan sulfate proteoglycans on the ovarian granulosa cell. *J Biol Chem* 268: 15579–15587, 1993.
- Tsuchida K. Activins, myostatin and related TGF-beta family members as novel therapeutic targets for endocrine, metabolic and immune disorders. *Curr Drug Targets Immune Endocr Metabol Disord* 4: 157–166, 2004.
- Tsuchida K. Targeting myostatin for therapies against muscle-wasting disorders. *Curr Opin Drug Discov Devel* 11: 487–494, 2008.
- Whittemore LA, Song K, Li X, Aghajanian J, Davies M, Girgenrath S, Hill JJ, Jalenak M, Kelley P, Knight A, Maylor R, O'Hara D, Pearson A, Quazi A, Ryerson S, Tan XY, Tomkinson KN, Veldman GM, Widom A, Wright JF, Wudyka S, Zhao L, Wolfman NM. Inhibition of myostatin in adult mice increases skeletal muscle mass and strength. *Biochem Biophys Res Commun* 300: 965–971, 2003.
- Wolfman NM, McPherron AC, Pappano WN, Davies MV, Song K, Tomkinson KN, Wright JF, Zhao L, Sebald SM, Greenspan DS, Lee SJ. Activation of latent myostatin by the BMP-1/tolloid family of metalloproteinases. *Proc Natl Acad Sci USA* 100: 15842–15846, 2003.
- Yang J, Zhao B. Postnatal expression of myostatin propeptide cDNA maintained high muscle growth and normal adipose tissue mass in transgenic mice fed a high-fat diet. *Mol Reprod Dev* 73: 462–469, 2006.
- Zhao B, Wall RJ, Yang J. Transgenic expression of myostatin propeptide prevents diet-induced obesity and insulin resistance. *Biochem Biophys Res Commun* 337: 248–255, 2005.

Original Article

Atelocollagen-mediated systemic administration of myostatin-targeting siRNA improves muscular atrophy in caveolin-3-deficient mice

Emi Kawakami,^{1†} Nao Kinouchi,^{1†} Taro Adachi,² Yutaka Ohsawa,³ Naozumi Ishimaru,⁴ Hideyo Ohuchi,² Yoshihide Sunada,³ Yoshio Hayashi,⁴ Eiji Tanaka¹ and Sumihare Noji^{2*}

¹Department of Orthodontics and Dentofacial Orthopedics, Institute of Health Bioscience, The University of Tokushima Graduate School, 3-18-15 Kuramoto, Tokushima 770-8504; ²Department of Life Systems, Institute of Technology and Science, The University of Tokushima, 2-1 Minami-Jyosanjima-cho, Tokushima 770-8506; ³Department of Neurology, Kawasaki Medical School, 577 Matsushima, Kurashiki City, Okayama 701-0192; and ⁴Department of Oral Molecular Pathology, Institute of Health Bioscience, The University of Tokushima Graduate School, 3-18-15 Kuramoto, Tokushima 770-8504, Japan

Small interfering RNA (siRNA)-mediated silencing of gene expression is rapidly becoming a powerful tool for molecular therapy. However, the rapid degradation of siRNAs and their limited duration of activity require efficient delivery methods. Atelocollagen (ATCOL)-mediated administration of siRNAs is a promising approach to disease treatment, including muscular atrophy. Herein, we report that ATCOL-mediated systemic administration of a myostatin-targeting siRNA into a caveolin-3-deficient mouse model of limb-girdle muscular dystrophy 1C (LGMD1C) induced a marked increase in muscle mass and a significant recovery of contractile force. These results provide evidence that ATCOL-mediated systemic administration of siRNAs may be a powerful therapeutic tool for disease treatment, including muscular atrophy.

Key words: atelocollagen, muscle, muscular dystrophy, myostatin, RNA interference.

Introduction

Myostatin (growth differentiation factor 8, GDF8) is a member of the transforming growth factor- β (TGF- β) superfamily of secreted growth factors (McPherron *et al.* 1997). A number of growth factors of this family have been shown to regulate cell growth and differentiation during development. Myostatin is unique among the members of the TGF- β superfamily because its expression is almost exclusively restricted to the skeletal muscle lineage.

Zhu *et al.* (2000) generated transgenic mice that expressed myostatin mutated at its cleavage site under the control of a muscle specific promoter creating a dominant negative myostatin. These mice exhibited a

significant (20–35%) increase in muscle mass that resulted from myofiber hypertrophy and not from myofiber hyperplasia. While, mice fully null for myostatin showed muscle masses that were nearly double that of normal muscle and this marked increase in muscle mass was associated with both hypertrophy and hyperplasia (McPherron *et al.* 1997). The difference in muscle mass seen in dominant negative myostatin and null myostatin mice likely results from incomplete dominance of dominant negative myostatin, so that dimerization and cleavage of normal myostatin is not fully blocked in dominant negative myostatin mice. So, lower levels of myostatin inhibition may affect hypertrophy, while higher levels of myostatin inhibition may be required to alter hyperplasia (Zhu *et al.* 2000). Thus, it appears that myostatin specifically downregulates skeletal muscle mass.

Because of its inhibitory role, myostatin downregulation may serve as a potentially important mechanism for treating diseases associated with muscle wasting and degeneration, such as muscular dystrophy. We recently demonstrated that myostatin inhibition induced by overexpression of the myostatin pro-domain prevented

*Author to whom all correspondence should be addressed.

Email: noji@bio.tokushima-u.ac.jp

[†]These authors contributed equally to this work.

Received 6 August 2010; revised 4 October 2010; accepted 4 October 2010.

© 2011 The Authors

Journal compilation © 2011 Japanese Society of Developmental Biologists

muscular atrophy and normalized intracellular myostatin signaling in a mouse model of limb-girdle muscular dystrophy 1C (LGMD1C) (Nishi *et al.* 2002). Furthermore, myostatin inhibition also suppressed muscular atrophy in caveolin-3-deficient mice that expressed a dominant-negative form of the caveolin-3 gene (Ohsawa *et al.* 2006). The dominant negative caveolin-3 mutation was a missense mutation (Pro104Leu) that was expressed under the control of the M-creatine kinase promoter (Sunada *et al.* 2001).

Duchenne muscular dystrophy (DMD) is an X-linked, lethal skeletal muscle disorder caused by mutations in the *dystrophin* gene (Bulfield *et al.* 1984; Yoshimura *et al.* 2007); it is a severe muscle wasting disorder that affects 1/3500 male births (Deconinck & Dan 2007). To date, there is no effective treatment for muscular dystrophy, although gene therapy could be a valuable approach to treating this disease. In a previous study, inhibition of myostatin using anti-myostatin blocking antibodies was employed in an effort to increase muscle mass (Bogdanovich *et al.* 2002). However, the generation of antibodies against recombinant target proteins was a time-consuming, labor-intensive approach.

Recently, RNA interference (RNAi) has emerged as an effective gene silencing method. RNAi refers to sequence-specific, post-transcriptional gene silencing mediated by approximately 22-nucleotide-long small interfering RNAs (siRNAs) generated from longer double-stranded RNAs (dsRNAs) in both plants and animals, ranging from flatworms to humans (Fire *et al.* 1998). RNAi-based approaches have increasingly been developed in which highly specific siRNAs designed to target disease-causing or disease-promoting genes are utilized without the induction of interferon synthesis or non-specific gene suppression (Elbashir *et al.* 2001; de Fougères *et al.* 2007). Magee *et al.* (2006) demonstrated that downregulation of myostatin expression via electroporation of a plasmid directing the expression of a short hairpin interfering RNA (shRNA) against myostatin led to a localized increase in skeletal muscle mass. For safety reasons, however, strategies using vector-based delivery systems may be of limited clinical use. Therefore, a more desirable approach would involve the direct application of active siRNAs *in vivo*.

Atelocollagen (ATCOL), a pepsin-treated type I collagen that lacks antigenicity-conferring telopeptides at its N and C termini, has been shown to promote the efficient delivery of chemically unmodified siRNAs to metastatic tumors *in vivo* (Minakuchi *et al.* 2004; Takeshita *et al.* 2005; Takeshita & Ochiya 2006). Based on its practical use as an siRNA delivery platform, we adapted an ATCOL-mediated oligonucleotide system to deliver a myostatin-targeting siRNA into muscle, and found that local or systemic administration of the

myostatin-targeting siRNA coupled with ATCOL led to a marked stimulation of muscle growth *in vivo* within a few weeks (Kinouchi *et al.* 2008). In the current study, we examined whether systemic administration of the myostatin-siRNA/ATCOL (Mst-siRNA/ATCOL) complex effectively silenced myostatin expression in LGMD1C mice, and whether it led to increased muscle mass and/or decreased muscle weakness. In the current study, we used the same myostatin-targeting siRNA reported previously (Magee *et al.* 2006), which is predicted to target myostatin mRNA not only in mice, but also in humans, rats, cows, macaques, and baboons.

Materials and methods

Systemic administration of the Mst-siRNA/ATCOL complex to skeletal muscles in LGMD1C mice

The Mst-siRNA and ATCOL complexes were prepared as follows. Equal volumes of siRNA solution (siRNA and 1× siRNA buffer, 40 μmol/L final concentration) and ATCOL (0.05% final concentration) were combined and mixed by vigorous pipetting. For systemic administration, the siRNA/ATCOL complex (200 μL) was introduced intravenously via orbital veins into 20-week-old LGMD1C mice at 0, 4, 7 and 14 days. As a negative control, scrambled siRNAs were injected into 20-week-old LGMD1C mice at 0, 4, 7 and 14 days.

Morphometric analyses

The masseter and quadriceps femoris muscle tissues were dissected 3 weeks after the first Mst-siRNA/ATCOL complex administration. The tissues were snap-frozen in liquid nitrogen-cooled isopentane and sectioned transversely (6 μm) at the center of the masseter and quadriceps femoris muscles using a cryostat (Leica Microsystems). Sections were stained with hematoxylin and eosin (H&E), and fiber sizes were determined by measuring the area of each transversal myofiber within a fixed area. Approximately 100 myofibers were measured for each tissue sample (six to eight fields/tissue section).

Contractile properties of Mst-siRNA/ATCOL complex-treated tibialis anterior (TA) muscles

The entire tibialis anterior (TA) muscle was removed with its tibial origin intact, and the distal portion of the TA tendon, together with its origin, were secured with a 5-0 silk suture. The TA was then mounted in a vertical tissue chamber and connected to a force transducer, UL-10GR (Minerva, Nagano, Japan), and a length servosystem, MM-3 (Narishige, Tokyo, Japan).

Electrical stimulations were applied using a SEN3301 (Nihon Kohden, Tokyo, Japan) through a pair of platinum wires placed on both sides of the muscle in physiological salt solution (150 mmol/L NaCl, 4 mmol/L KCl, 2 mmol/L CaCl₂, 1 mmol/L MgCl₂, 5.6 mmol/L glucose, 5 mmol/L Hepes, pH 7.4, and 0.02 mmol/L D-tubocurarine). Muscle fiber length was adjusted incrementally using a micropositioner until peak isometric twitch force responses were obtained (optimal fiber length [L_0]). Maximal tetanic force (P_0) was assessed by stimulation frequencies of 125 pulses/s delivered in 500 ms duration trains with 2 min intervals between each train. After two measurements were taken, the stimulated muscles were weighted after the tendon and bone attachments were removed. All forces were normalized to the physiological cross-sectional area (pCSA), the latter estimated on the basis of the following formula: muscle wet weight (in mg)/(L_0 [in mm] \times 1.06 [in mg/mm³]). The estimated pCSA was used to determine specific tetanic force, and the muscle was quickly frozen in liquid nitrogen-cooled isopentane for morphometric analysis.

Statistical analyses

Error bars indicate standard deviation of the mean. * indicates $P < 0.01$ or $P < 0.05$ in a Student's *t* test.

Results

The Mst-siRNA/ATCOL complex can stabilize and produce a long-term gene silencing effect

In initial experiments to evaluate the persistence and spread of siRNA/ATCOL complexes (100 μ L), we injected a BLOCK-IT Alexa Fluor Red Fluorescent Oligo (10 μ mol/L) in the masseter muscle of 20-week-old C57BL/6 mice. Mice were killed at 2 weeks, tissue samples were dissected, and Alexa Fluor Red Fluorescent Oligo expression was assessed under conditions identical to those used in myostatin gene transfer experiments. As expected, Alexa Fluor Red Fluorescent Oligo expression was detected near the sites of injection with an uneven distribution pattern across the tissue (Fig. 1, right panel). These observations suggested that the ATCOL and siRNA formed a stable complex capable of producing an efficient, long-term gene silencing effect.

Intravenous administration of myostatin-targeting siRNAs with ATCOL specifically repressed muscle atrophy in LGMD1C mice

Based on our observation that ATCOL formed stable complexes with siRNAs capable of long-term gene

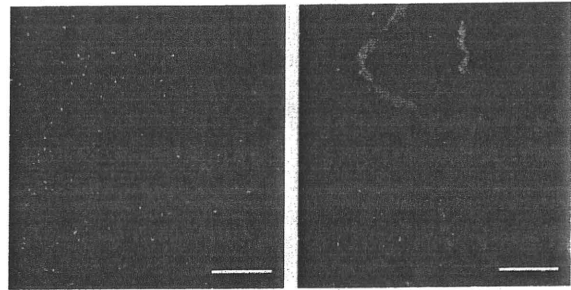


Fig. 1. Persistence and spread of an siRNA/atelocollagen (ATCOL, AteloGene Koken, Tokyo) complex following injection into the masseter muscle. A BLOCK-IT Alexa Fluor Red Fluorescent Oligo (10 μ mol/L final concentration, Invitrogen) and ATCOL (100 μ L) complex was injected into the masseter muscle of 20-week-old C57BL/6 mice. Gene expression from the BLOCK-IT Alexa Fluor Red Fluorescent Oligo/ATCOL complex injected in masseter muscle was assessed 2 weeks post-injection. Sections were examined following hematoxylin and eosin (H&E) staining (left) and serial section immunofluorescence to detect Alexa Fluor Red-positive cells (right). As expected, the Alexa Fluor Red Fluorescent Oligo expression was not evenly distributed across the tissue, and the majority of expression was located near the injection sites. Images were captured at 400 \times magnification. Scale bar, 100 μ m.

silencing, we administered Mst-siRNA/ATCOL or control scrambled siRNA/ATCOL complexes intravenously into 20-week-old LGMD1C mice at 0, 4, 7, and 14 days (Fig. 2A). Strikingly, we observed the enlargement of a number of skeletal muscles, including the lower limbs, masseters, and more in mice treated with Mst-siRNA/ATCOL (Fig. 2B). Since the changes in the lower limb muscles were the most pronounced, we used them for further analyses. Indeed, we also observed a significant increase in muscle fiber size at 3 weeks after the first administration in mice treated with Mst-siRNA/ATCOL (Fig. 2C).

These results indicated that intravenous administration of a myostatin-targeting siRNA with ATCOL specifically induced muscle hypertrophy in LGMD1C mice. The results were expressed as a ratio of the internal control and were analyzed statistically. Mst-siRNA/ATCOL-treated muscles ($18.64 \pm 4.18 \mu\text{m}$) were significantly larger than control muscles ($15.49 \pm 3.12 \mu\text{m}$) ($P < 0.0001$, $n = 100$). Histometric analysis showed that the myofibril sizes of quadriceps muscles treated with the Mst-siRNA/ATCOL complex were significantly larger than those of control quadriceps muscles (Fig. 2C,D). Examination of the sizes of 100 myofibers from each group showed that the Mst-siRNA/ATCOL-treated myofibril population exhibited a shift from smaller to larger sized fibers; the average myofibril size for Mst-siRNA/ATCOL-treated muscle was increased

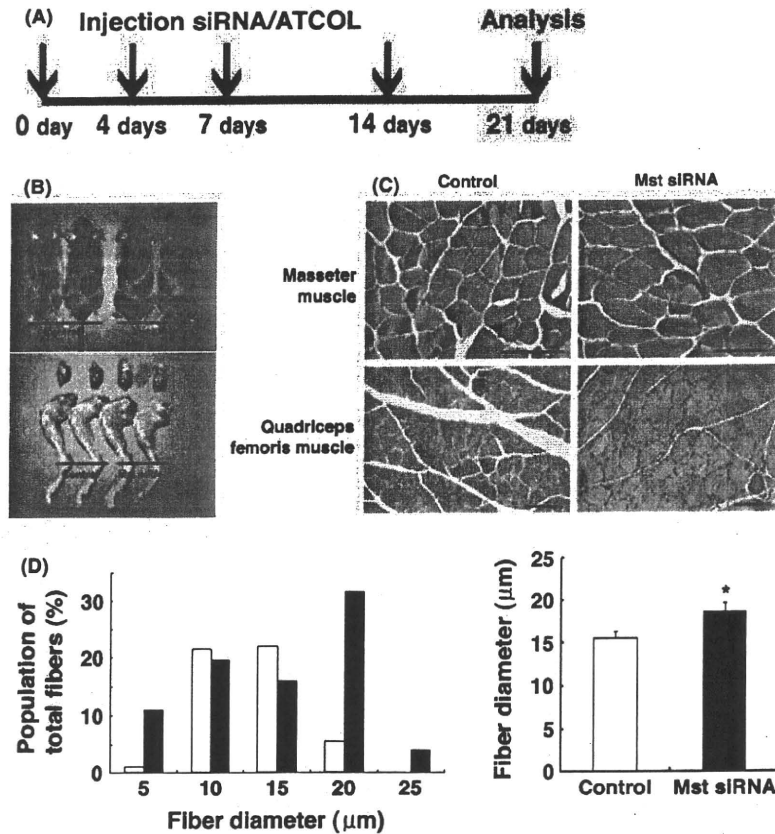


Fig. 2. Systemic administration of the Mst-siRNA/ATCOL complex led to increased skeletal muscle mass and fiber size in LGMD1C mice via inhibition of myostatin expression. In the experiments depicted in (A–C), Mst-siRNA (40 $\mu\text{mol/L}$ final concentration) was mixed with ATCOL according to the manufacturer's instructions. (A) Time course analysis. Twenty-week-old male or female LGMD1C mice were anesthetized with Nembutal (25 mg/kg i.p.), and the Mst-siRNA/ATCOL complex (40 $\mu\text{mol/L}$ in a 200 μL volume) was introduced intravenously via orbital veins at 0, 4, 7, and 14 days ($n = 3$). As a negative control, scrambled siRNAs were injected into LGMD1C mice. At 3 weeks after the first administration, the quadriceps muscles on both sides were harvested and processed for analysis. (B) Photographs of mice (upper panels) and lower limbs (lower panels). An increase in muscle mass was observed in the Mst-siRNA/ATCOL-treated (right), but not in control mice (left). (C) H&E staining of control (left) and Mst-siRNA/ATCOL-treated (right) masseter or quadriceps femoris muscle. Images of the masseter and quadriceps femoris were captured at 400x and 200x, respectively. Scale bar, 50 μm . (D) Distribution of the myofibril sizes of control (white bars) and Mst-siRNA/ATCOL-treated (black bars) quadriceps muscles. The right panel shows the average myofibril size ($15.49 \pm 3.12 \mu\text{m}$ vs. $18.64 \pm 4.18 \mu\text{m}$, respectively; $n = 100$; $P < 0.01$). The graphical representation of the data uses the following convention: mean \pm SD. Mst-siRNA/ATCOL-treated muscles and mice are shown in black; control muscles and mice are shown in white. National Institute of Health (NIH) Image (NIH) software was used for morphometric measurements.

by approximately 1.2-fold relative to control muscle (Fig. 2D).

Hypertrophied Mst-siRNA/ATCOL-treated LGMD1C muscle fibers exhibit significantly improved contractile force generation

First, we tested the grip strength of mice before and after treatment. There were no statistically significant differences in the grip strength before and after treatment (Fig. 3D). We also evaluated the contractile properties of

Mst-siRNA/ATCOL-treated LGMD1C muscle (Fig. 3C). We did not identify any statistically significant differences in the wet weights of Mst-siRNA/ATCOL-treated and untreated LGMD1C muscle. Unexpectedly, the specific force of untreated LGMD1C muscle was much lower than that of Mst-siRNA/ATCOL-treated LGMD1C muscle (Fig. 3A,B). We analyzed the specific force generated by tetanic stimulation (150 Hz) of TA muscles from LGMD1C mice treated with ATCOL-based control scrambled siRNAs or Mst-siRNA (0.568 ± 0.293 vs. $0.041 \pm 0.351 \text{ N/cm}^2$, respectively; $n = 4$; $P < 0.05$).

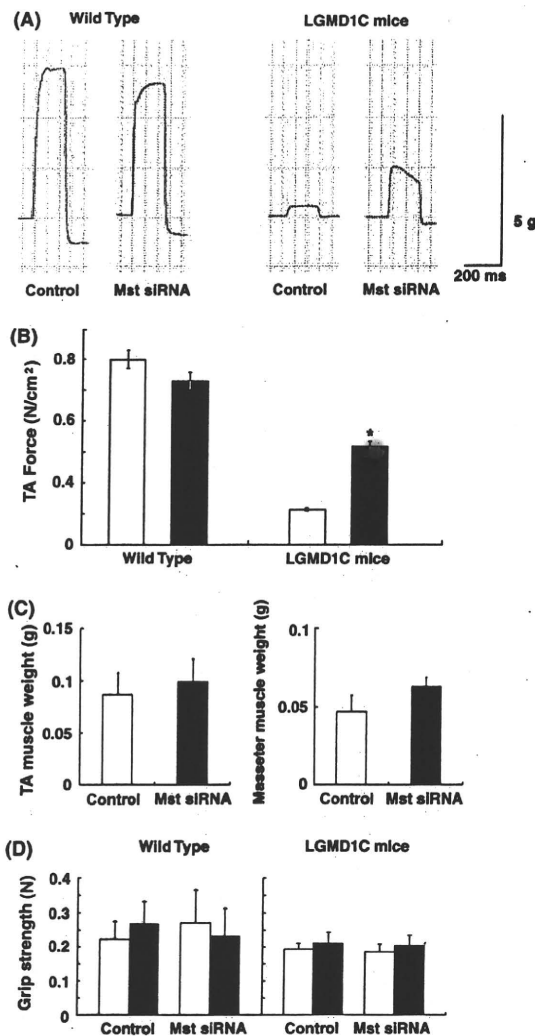


Fig. 3. Mst-siRNA/ATCOL-treated fibers exhibited significantly improved contractile force generation. (A) Specific force generated by tetanic stimulation (150 Hz) of TA muscles from wild-type or LGMD1C mice treated with ATCOL-based control scrambled siRNAs or Mst-siRNA. (B) The specific force of untreated LGMD1C muscle (□) was much lower than that of Mst-siRNA/ATCOL-treated LGMD1C muscle (■) (0.569 ± 0.293 N/cm² vs. 0.041 ± 0.351 N/cm², respectively; $n = 4$; $P < 0.05$). In contrast, in wild-type mice, the specific force was not different between untreated muscle and Mst-siRNA/ATCOL-treated muscle (0.888 ± 0.588 N/cm² vs. 0.925 ± 0.828 N/cm²; $n = 3$). (C) There were no statistically significant differences in wet weights between untreated muscles and Mst-siRNA/ATCOL-treated muscles. (D) There were no statistically significant differences in grip strength between pre-treated mice (□) and after Mst-siRNA/ATCOL-treated mice (■).

Although wild-type fibers have been found to be hypertrophied (Kinouchi *et al.* 2008), the present results did not show a significant difference between the contractile

force generated by Mst-siRNA/ATCOL-treated and untreated wild-type muscle (0.888 ± 0.588 vs. 0.925 ± 0.828 N/cm²; $n = 3$). As shown in Figure 2D, histogram analysis demonstrated a shift to the right in the fiber distribution of Mst-siRNA/ATCOL-treated LGMD1C muscle relative to that of untreated LGMD1C muscle; larger caliber fibers were dominant, reflecting hypertrophy of Mst-siRNA/ATCOL-treated muscle fibers. Thus, hypertrophied Mst-siRNA/ATCOL-treated LGMD1C muscle fibers exhibited improved contractile force generation, but the increase in muscle weight did not correlate with increased force generation.

We previously reported that local and systemic administration of siRNA against myostatin coupled with ATCOL markedly stimulated muscle growth *in vivo* within a few weeks (Kinouchi *et al.* 2008), and that ATCOL-based gene therapy was associated with low immunogenicity. As expected, we did not observe any signs or symptoms suggestive of health problems during the experimental period of the current study.

Discussion

In the current study, we intravenously administered a myostatin-targeting siRNA with ATCOL and analyzed the relationship between the extent of Mst-siRNA/ATCOL expression and the recovery of contractile force in LGMD1C muscles. Histogram analysis further demonstrated that the myofibril size distribution of Mst-siRNA/ATCOL-treated LGMD1C muscle fibers was shifted from smaller to larger sized fibers relative to control muscle fibers. We found that treatment of LGMD1C mice with the Mst-siRNA/ATCOL complex led to a significant increase in skeletal muscle mass and enhanced contractile force, similar to that reported previously with a myostatin blockade of dystrophic muscle (Bogdanovich *et al.* 2002).

There was no statistically significant difference in muscle weight between control and Mst-siRNA/ATCOL-treated muscles. It appeared that muscle weight did not correlate with force generation. Thus, hypertrophied Mst-siRNA-positive LGMD1C fibers seemed to greatly improve contractile force generation. Notably, the level of contractile force was dramatically improved by approximately 60% in Mst-siRNA/ATCOL-treated wild-type muscles relative to control muscles. Although the underlying molecular mechanisms by which Mst-siRNA/ATCOL treatment leads to increased contractile force remain to be determined, the current results are encouraging in that the function of caveolin-3-deficient muscles might be greatly improved. These findings are significant because the recovery of absolute maximal force and specific tetanic force are barometers of amelioration (Yoshimura *et al.* 2007).

To our knowledge, the results of the current study are the first to quantitatively and qualitatively demonstrate that *in vivo* myostatin siRNA gene transfer may serve as an effective treatment for muscular dystrophy. The potential benefit of myostatin siRNA gene therapy lies in the treatment of skeletal muscle waste in conditions such as muscular dystrophies (Bogdanovich *et al.* 2002), cachexia and HIV infection in advance of new therapies (Gonzalez-Cadavid & Bhasin 2004; Frimel *et al.* 2005). Although myostatin siRNA gene therapy would not correct the underlying pathophysiology of these diseases, it would counterbalance the effects by stimulating myofiber growth. The ease of administration of the myostatin-siRNA/ATCOL complex combined with its muscle-growth effect makes it a clinically valuable method of fighting against muscle atrophy. However, a strategy for the clinical use of this gene transfer method for human DMD patients requires further testing. Differences between humans and mice, including muscle size, life span and biological properties, should be taken into consideration (Yoshimura *et al.* 2007). In tumor-bearing mice, it was reported that ATCOL distributed siRNAs against luciferase to normal liver, lung, spleen and kidney tissues, as well as to bone-metastatic lesions (Takeshita *et al.* 2005). ATCOL was also reported to display low-toxicity and low-immunogenicity when it is transplanted *in vivo* (Ochiya *et al.* 2001; Sano *et al.* 2003).

Taken together, the results of the present study demonstrate that administration of siRNAs with ATCOL may be a promising therapeutic tool not only for muscular diseases, but also for other genetic diseases. The results of the current study indicate that treatment with Mst-siRNA/ATCOL led to an increase in muscle mass and functional recovery in the absence of obvious adverse effects in LGMD1C mice. The current study also provides evidence of ATOL-mediated delivery of siRNA to skeletal muscle. Therefore, ATCOL-mediated administration of siRNAs represents a powerful new tool for future therapeutic use in the treatment of diseases, including muscular atrophy.

Acknowledgments

We thank Nami Naoe, Masahiro Fujino and Tadashi Okada (Division of Neurology, Kawasaki Medical School) for expert technical assistance. This work was supported by an intramural research grant (20B-13) for neurological and psychiatric disorders of NCNP and a research grant (H20-018) for comprehensive research on disability, health and welfare from the Ministry of Health, Labour and Welfare, a Grant for Research on Psychiatric and Neurological Diseases and Mental Health from the Ministry of Health, Labour and Welfare

of Japan (15131301) to Y.O., funding from JSPS KAKENHI (14370212) to YS and Research Project Grants from Kawasaki Medical School (15-115B and 16-601) to Y.O. and Y.S.

References

- Bogdanovich, S., Krag, T. O., Barton, E. R., Morris, L. D., Whitemore, L. A., Ahima, R. S. & Khurana, T. S. 2002. Functional improvement of dystrophic muscle by myostatin blockade. *Nature* **420**, 418–421.
- Bulfield, G., Siller, W. G., Wight, P. A. & Moore, K. J. 1984. X chromosome-linked muscular dystrophy (mdx) in the mouse. *Proc. Natl Acad. Sci. USA* **81**, 1189–1192.
- Deconinck, N. & Dan, B. 2007. Pathophysiology of duchenne muscular dystrophy: current hypotheses. *Pediatr. Neurol.* **36**, 1–7.
- de Fougerolles, A., Vornlocher, H. P., Maraganore, J. & Lieberman, J. 2007. Interfering with disease: a progress report on siRNA-based therapeutics. *Nat. Rev. Drug. Discov.* **6**, 443–453.
- Elbashir, S. M., Harborth, J., Lendeckel, W., Yalcin, A., Weber, K. & Tuschl, T. 2001. Duplexes of 21-nucleotide RNAs mediate RNA interference in cultured mammalian cells. *Nature* **411**, 494–498.
- Fire, A., Xu, S., Montgomery, M. K., Kostas, S. A., Driver, S. E. & Mello, C. C. 1998. Potent and specific genetic interference by double-stranded RNA in *Caenorhabditis elegans*. *Nature* **391**, 806–811.
- Frimel, T. N., Kapadia, F., Gaidosh, G. S., Li, Y., Walter, G. A. & Vandenberg, K. 2005. A model of muscle atrophy using cast immobilization in mice. *Muscle Nerve* **32**, 672–674.
- Gonzalez-Cadavid, N. F. & Bhasin, S. 2004. Role of myostatin in metabolism. *Curr. Opin. Clin. Nutr. Metab. Care* **7**, 451–457.
- Kinouchi, N., Ohsawa, Y., Ishimaru, N., Ohuchi, H., Sunada, Y., Hayashi, Y., Tanimoto, Y., Moriyama, K. & Noji, S. 2008. Atelocollagen-mediated local and systemic administrations of myostatin-targeting siRNA increase skeletal muscle mass. *Gene Ther.* **15**, 1126–1130.
- Magee, T. R., Artaza, J. N., Ferrini, M. G., Vernet, D., Zuniga, F. I., Cantini, L., Reisz-Porszasz, S., Rajfer, J. & Gonzalez-Cadavid, N. F. 2006. Myostatin short interfering hairpin RNA gene transfer increases skeletal muscle mass. *J. Gene Med.* **8**, 1171–1181.
- McPherron, A. C., Lawler, A. M. & Lee, S. J. 1997. Regulation of skeletal muscle mass in mice by a new TGF- β superfamily member. *Nature* **387**, 83–90.
- Minakuchi, Y., Takeshita, F., Kosaka, N., Sasaki, H., Yamamoto, Y., Kouno, M., Honma, K., Nagahara, S., Hanai, K., Sano, A., Kato, T., Terada, M. & Ochiya, T. 2004. Atelocollagen-mediated synthetic small interfering RNA delivery for effective gene silencing *in vitro* and *in vivo*. *Nucleic Acids Res.* **32**, e109.
- Nishi, M., Yasue, A., Nishimatu, S., Nohno, T., Yamaoka, T., Itakura, M., Moriyama, K., Ohuchi, H. & Noji, S. 2002. A missense mutant myostatin causes hyperplasia without hypertrophy in the mouse muscle. *Biochem. Biophys. Res. Commun.* **293**, 247–251.
- Ochiya, T., Nagahara, S., Sano, A., Itoh, H. & Terada, M. 2001. Biomaterials for gene delivery: atelocollagen-mediated controlled release of molecular medicines. *Curr. Gene Ther.* **1**, 31–52.
- Ohsawa, Y., Hagiwara, H., Nakatani, M., Yasue, A., Moriyama, K., Murakami, T., Tsuchida, K., Noji, S. & Sunada, Y. 2006.

- Muscular atrophy of caveolin-3-deficient mice is rescued by myostatin inhibition. *J. Clin. Invest.* **116**, 2924–2934.
- Sano, A., Maeda, M., Nagahara, S., Ochiya, T., Honma, K., Itoh, H., Miyata, T. & Fujioaka, K. 2003. Atelocollagen for protein and gene delivery. *Adv. Drug Deliv. Rev.* **55**, 1651–1677.
- Sunada, Y., Ohi, H., Hase, A., Ohi, H., Hosono, T., Arata, S., Higuchi, S., Matsumura, K. & Shimizu, T. 2001. Transgenic mice expressing mutant caveolin-3 show severe myopathy associated with increased nNOS activity. *Hum. Mol. Genet.* **10**, 173–178.
- Takeshita, F., Minakuchi, Y., Nagahara, S., Honma, K., Sasaki, H., Hirai, K., Teratani, T., Namatame, N., Yamamoto, Y., Hanai, K., Kato, T., Sano, A. & Ochiya, T. 2005. Efficient delivery of small interfering RNA to bone-metastatic tumors by using atelocollagen in vivo. *Proc. Natl Acad. Sci. USA* **102**, 12177–12182.
- Takeshita, F. & Ochiya, T. 2006. Therapeutic potential of RNA interference against cancer. *Cancer Sci.* **97**, 689–696.
- Yoshimura, M., Sakamoto, M., Ikemoto, M., Mochizuki, Y., Yuasa, K., Miyagoe-Suzuki, Y. & Takeda, S. 2007. AAV vector-mediated microdystrophin expression in a relatively small percentage of mdx myofibers improved the mdx phenotype. *Mol. Ther.* **15**, 320–329.
- Zhu, X., Hadhazy, M., Wehling, M., Tidball, J. G. & McNally, E. M. 2000. Dominant Negative myostatin produces hypertrophy without hyperplasia in muscle. *FEBS Lett.* **474**, 71–75.

Chapter 20

Antisense Oligo-Mediated Multiple Exon Skipping in a Dog Model of Duchenne Muscular Dystrophy

Toshifumi Yokota, Eric Hoffman, and Shin'ichi Takeda

Abstract

Exon skipping is currently one of the most promising molecular therapies for Duchenne muscular dystrophy (DMD). We have recently developed multiple exon skipping targeting exons 6 and 8 in dystrophin mRNA of canine X-linked muscular dystrophy (CXMD), an animal model of DMD, which exhibits severe dystrophic phenotype in skeletal muscles and cardiac muscle. We have induced efficient exon skipping both in vitro and in vivo by using cocktail antisense 2'-O-methyl oligonucleotides (2'OMePS) and cocktail phosphorodiamidate morpholino oligomers (morpholinos, or PMOs) and ameliorated phenotype of dystrophic dogs by systemic injections. The multiple exon skipping (double exon skipping) shown here provides the prospect of choosing deletions that optimize the functionality of the truncated dystrophin protein for DMD patients by using a common cocktail that could be validated as a single drug and also potentially applicable for more than 90% of DMD patients.

Key words: Multiple exon skipping, Morpholinos (phosphorodiamidate morpholino oligomers), 2'-O-methylated antisense oligomers (phosphorothioate), Dystrophic dogs (canine X-linked muscular dystrophy), Duchenne/Becker muscular dystrophies

1. Introduction

Duchenne muscular dystrophy (DMD), a progressive and fatal X-linked myopathy, and its milder form, Becker muscular dystrophy (BMD), are caused by mutations in the *DMD* gene (1). Exon skipping using antisense oligonucleotides (AOs) is currently one of the most promising molecular therapies for DMD (2–4). Synthetic derivatives of nucleic acids have been designed and synthesized, where the backbone of RNA and DNA is replaced with other chemistries. One uses a morpholino backbone phosphorodiamidate morpholino oligomers (morpholinos, or PMOs) developed by AVI BioPharma, Portland, Oregon.

Recently, we have successfully induced dystrophin expression by using morpholino-mediated systemic multiple exon skipping and ameliorated dystrophic pathology in dogs (5). Another antisense chemistry 2'-O-methylated phosphorothioate (2'OMePS) has been also shown to effectively induce dystrophin expression systemically in mice in vivo (6).

The canine X-linked muscular dystrophy (CXMD) model contains a point mutation within the acceptor splice site of exon 7. This leads to exclusion of exon 7 from the mRNA transcript (7, 8). To restore the open reading frame, at least two further exons (exons 6 and 8) must be skipped (multiple exon skipping, or multiexon-skipping). Therefore, it is more challenging to rescue dystrophic dogs with exon-skipping strategy. Here, we summarize the method and protocol of antisense-mediated exon skipping in vitro and in vivo in dystrophic CXMD dogs.

2. Materials

2.1. Design of Antisense Oligos

1. Web sites for exonic splicing enhancer ESE targeting. ESE finder [<http://rulai.cshl.edu/cgi-bin/tools/ESE3/csefinder.cgi?process=home>] and Rescue ESE [<http://genes.mit.edu/burgelab/rescue-cse/>].

2.2. Transfection of Antisense 2'OMePS into Dog Myoblasts

1. Dulbecco's modified Eagle's medium (DMEM) (Gibco, Bethesda, MD, USA) supplemented with 10% fetal bovine serum (FBS, HyClone, Ogden, UT, USA).
2. 0.25% Trypsin and 1 mM ethylenediamine tetraacetic acid (EDTA) (Gibco).
3. Teflon cell scrapers (Fisher, Waltham, MA, USA).
4. Ham's F-10 nutrient mixture with HEPES (Gibco) (9).
5. Fetal calf serum (FCS) (Gibco).
6. Human recombinant basic fibroblast growth factor (bFGF) (Sigma-Aldrich, Natick, MA, USA).
7. Penicillin (200 U/mL) and streptomycin (200 µg/mL) (Sigma-Aldrich).
8. AOs (2'OMePS) (Eurogentec, Liège, Belgium) against exons 6 and 8 of the canine dystrophin gene. Ex6A (GUU GAUUGUCGGACCCAGCUCAGG), Ex6B (ACCUAUGA CUGUGGAUGAGAGCGUU), and Ex8A (CUUCCUGG AUGGCUUCA AUGCUCAC).
9. Lipofectin (Invitrogen, Carlsbad, CA, USA).
10. 2% Horse serum (Gibco).
11. Six-well plates (IWAKI, Funabashi, Japan).

12. Opti-MEM (Gibco).
13. Culture dish (10, 15 cm noncoat and 10, 15 cm collagen coat) (IWAKI).
14. Phosphate buffer saline (PBS).
15. Human recombinant insulin (10 mg/mL) (Sigma-Aldrich).
16. Proliferation medium: Nutrient Mixture F-10 Ham (Ham's F-10; developed by Ham et al. for mammalian cell proliferation (9)) supplemented with 200 U/mL penicillin, 200 µg/mL streptomycin, 2.5 ng/mL bFGF, and 20% FBS.
17. Differentiation medium: DMEM supplemented with 200 U/mL penicillin, 200 µg/mL streptomycin, and 10 µg/mL insulin.

**2.3. Intramuscular
Injections of Antisense
Oligos in Dogs**

1. CXMD dogs and wild type littermates.
2. Antisense morpholinos (Gene-tools, Philomath, OR, USA) against exons 6 and 8 of the dog dystrophin gene. Ex6A (GTTGATTGTCTGGACCCAGCTCAGG), Ex6B (ACCTATGACTGTGGATGAGAGCGTT), and Ex8A (CTTCCTGGATGGCTTCAATGCTCAC) (see Note 1).
3. Saline (Ohtsuka-Pharmaceutical, Tokyo, Japan).
4. 27G Needles (TERUMO, Tokyo, Japan).
5. Thiopental sodium (Mitsubishi Tanabe Pharma, Osaka, Japan).
6. Isoflurane (Abbott laboratories, Chicago, IL, USA).
7. Butorphanol tartrate (Bedford Laboratories, Bedford, OH, USA).
8. Gauze (Johnson and Johnson, New Brunswick, NJ, USA).
9. Pledget (Johnson and Johnson).
10. Veterinary surgical instruments: forceps, scalpels, scissors, suture needles, threads, and needle holders (Mizuho, Narashino, Japan).
11. Povidone iodine (Meiji Seika, Tokyo, Japan).
12. Heparin sodium (Fuji Pharmaceutical, Tokyo, Japan).
13. Surgical glove (Ansell, Red bank, NJ, USA).
14. Surgical drape (Nagai Leben, Tokyo, Japan).
15. Sepham antibiotics (Cefamezine or Syncl) (Astellas, Tokyo, Japan, or Asahi-kasei, Tokyo, Japan).

**2.4. Systemic
Injections of Antisense
Morpholinos**

1. CXMD dogs and wild-type littermates.
2. Syringe infusion pump (Muromachi, Tokyo, Japan).
3. 22G Indwelling needles (TERUMO).
4. 50 mL syringe (TERUMO).

5. Antisense morpholinos (Gene-tools) against exons 6 and 8 of the dog dystrophin gene. Ex6A (GTTGATTGTCGGA CCCAGCTCAGG), Ex6B (ACCTATGACTGTGGATGA GAGCGTT), and Ex8A (CTTCCTGGATGGCTTCAATG CTCAC).

2.5. RNA Extraction

1. Eppendorf tubes (Eppendorf, Hamburg, Germany).
2. Trizol (Invitrogen).
3. Chloroform (Sigma-Aldrich).
4. Isopropanol (Sigma-Aldrich).
5. 75% Ethanol (Sigma-Aldrich).

2.6. RT-PCR

1. One-Step RT-PCR kit (Qiagen, Venlo, The Netherlands).
2. Forward primer in exon 5: CTGACTCTTGGTTGA TTTGGA (Invitrogen).
3. Reverse primer in exon 10: TGCTTCGGTCTCTGTCAATG (Invitrogen).
4. RNAsin (Promega, Madison, WI, USA).

2.7. cDNA Sequencing

1. Gel extraction kit (Qiagen).
2. BigDye® Terminator v3.1 Cycle Sequencing Kit (Applied Biosystems, Foster City, CA, USA).
3. ExoSap-IT® (USB, Santa Clara, CA, USA).
4. MicroAmp® Reaction Plates (Applied Biosystems).
5. Qiagen gel extraction kit (Qiagen).
6. Hidi-formamide (Applied Biosystems).
7. ABI 3130 Genetic Analyzer (Applied Biosystems).

2.8. Muscle Sampling from Necropsy of Dogs

1. Tragacanth gum (Sigma-Aldrich).
2. Isopentane (Sigma-Aldrich).
3. Liquid nitrogen.
4. Cork disks (Iwai-kagaku, Tokyo, Japan).
5. Dry ice.

2.9. Immunostaining for Dog Muscles

1. Poly-l-lysine-coated slides (Fisher, Hampton, NH, USA).
2. Cover glasses (Fisher).
3. Cryostat Microsystem cm1900 (Leica, Wetzlar, Germany).
4. Dystrophin antibodies including DYS1 and DYS2 (Novocastra, Newcastle, UK).
5. Alexa 594 goat antimouse IgG₁, Alexa 594 goat antimouse IgG₂, highly cross-absorbed (Invitrogen).
6. DAPI containing mounting agent (Invitrogen).
7. Goat serum (Invitrogen).

8. Moisture chamber (Scientific Devise Laboratory, Des Plaines, IL, USA).
9. Chamber slide (Lab-tek, Naperville, IL).
10. 4% Paraformaldehyde (PFA).

2.10. Western Blotting from Dog Muscles

1. Lysis buffer: 75 mM Tris-HCl (pH 6.8), 10% SDS, 10 mM EDTA, and 5% 2-mercaptoethanol.
2. Bradford reagent (Bio-Rad, Hercules, CA, USA).
3. Bovine serum albumin (BSA) (Sigma-Aldrich).
4. 2× Laemmli SDS-loading buffer: 0.1 M Tris-HCl (pH 6.6), 2% (w/v) SDS, 2% (0.28 M) beta-mercaptoethanol, 20% glycerol, 0.01% bromophenol blue.
5. Ready-made 5% resolving SDS gels (Bio-Rad).
6. PVDF membrane (GE, Fairfield, CT, USA).
7. Transfer buffer (10×): 250 mM of Tris-Base, 1,920 mM of Glycine.
8. Transfer buffer (1×): 10% 10× buffer, 20% methanol.
9. Dystrophin antibodies including DYS1 and DYS2 (Novocastra) and desmin antibody (Abcam, Cambridge, MA, USA).
10. ECL plus kit (GE).
11. ECL and autoradiography film (GE).
12. ImageJ software (NIH, Bethesda, MD, USA).

2.11. Clinical Grading of Dogs

1. Video camera.
2. Stop watch.

3. Methods

3.1. Design of Antisense Oligos

1. Identify ESE sites in exons using Rescue ESE and ESEfinder.
2. Design antisense sequences to target ESEs of exon 6 (Ex6A) and exon 8 (Ex8A), or exon/intron boundary between exon 6 and intron 6 (Ex6B), or between exon 8 and intron 8 (Ex8B) (see Note 2).
3. Select antisense oligonucleotide chemistries. 2'OMePS is preferred for myoblast experiment (see Note 3). PMOs are used for in vivo studies (see Note 1).

3.2. Transfection of Antisense 2'OMePS into Dog Myoblasts

1. Use standard preplating method to obtain primary myoblast cells from neonatal CXMD dogs (10).
2. Culture WT or CXMD myoblasts (1.5×10^5 cells) in growth medium containing F-10, FCS (20%), bFGF (2.5 ng/mL),